The Relationship Between Frictional Resistance and Roughness for Surfaces Smoothed by Sanding

Michael P. Schultz
Department of Naval Architecture & Ocean Engineering,
United States Naval Academy,
Annapolis, MD 21402

An experimental investigation has been carried out to document and relate the frictional resistance and roughness texture of painted surfaces smoothed by sanding. Hydrodynamic tests were carried out in a towing tank using a flat plate test fixture towed at a Reynolds number (Re_L) range of $2.8\times10^6-5.5\times10^6$ based on the plate length and freestream velocity. Results indicate an increase in frictional resistance coefficient (C_F) of up to 7.3% for an unsanded, as-sprayed paint surface compared to a sanded, polished surface. Significant increases in C_F were also noted on surfaces sanded with sandpaper as fine as 600-grit as compared to the polished surface. The results show that, for the present surfaces, the centerline average height (R_a) is sufficient to explain a large majority of the variance in the roughness function (ΔU^+) in this Reynolds number range.
[DOI: 10.1115/1.1459073]

Introduction

Many practical engineering applications involve turbulent flows over surfaces that have been smoothed by sanding. Examples range from sailing hulls to models for wind and water tunnels. While a great deal of drag data has been generated for sandgrain roughness (most notably Nikuadse's experiments on monodisperse, closely-packed sand [1]), there are few reliable data for sanded surfaces in which the surface is well documented. This is noteworthy since sanded surfaces form a much larger presence in engineering applications than sandgrain roughness. The purpose, therefore, of the present investigation is to study the frictional resistance of sanded surface roughness.

A large body of basic research has focused on the effect of surface roughness on frictional resistance. Hama [2], Ligrani and Moffat [3], Krogstad and Antonia [4] and many others have investigated the structure of the turbulent boundary layer over rough surfaces. Raupach et al. [5] give a review of much of this work. Studies focusing on the frictional resistance of ship bottom paints have also been made. Grigson [6], Townsin et al. [7], Musker [8], and Lewkowicz and Musker [9] have all investigated these surfaces, and their results indicate that as-sprayed antifouling coatings have significantly higher frictional resistance than a smooth surface. An entire workshop was devoted to the subject of ship hull roughness and drag [10]. However, most of the research into the drag on marine paints has centered on predicting the economic penalty of hull roughness on commercial ships, where sanding is unfeasible.

The mean velocity profile in a turbulent boundary layer can be expressed as:

$$U^+=\frac{1}{\kappa}\ln(y^+)+B+2\omega(y/\delta)\Pi/\kappa \tag{1}$$

Clauser [11] noted that for rough wall flows, the log-law intercept is shifted downward and that the shift correlates with k^+, the roughness Reynolds number, defined as the ratio of the roughness length scale, k, to the viscous length scale, ν/U_τ. This downward shift, ΔU^+, called the roughness function, can be used to express the mean velocity profile for rough wall flows:

$$U^+=\frac{1}{\kappa}\ln(y^+)+B-\Delta U^+ +2\omega(y/\delta)\Pi/\kappa \tag{2}$$

Hama [2] showed that by evaluating Eqs. (2) and (3) at $y=\delta$, the roughness function could be found by subtracting the rough wall intercept from the smooth wall intercept, B, at the same value of Re_{δ^*}. The roughness function therefore can be expressed as:

$$\Delta U^+=\left(\sqrt{\frac{2}{c_f}}\right)_S-\left(\sqrt{\frac{2}{c_f}}\right)_R \tag{3}$$

It should be noted that Eq. (3) is only valid provided both Π and the velocity defect profile are the same for the rough and smooth walls. The experimental evidence for this is somewhat contradictory. Some research indicates that surface roughness increases Π (e.g. [4]) and alters the velocity defect profile (e.g. [12]), while other studies (e.g. [13]) indicate that these are unchanged by roughness. In the present study, no mean velocity profiles were made. Therefore, the determination of the roughness function required the explicit assumption that Π and the velocity defect profile are unchanged by the roughness to be made. Future studies are planned that will include measurements of the mean velocity profiles over these sanded surfaces.

A universal roughness function for a given class of surfaces can be defined if k is related directly to the surface profile. Nikuradse's [1] pipe flow experiments on closely-packed, uniform sand roughness show that this roughness type has a universal roughness function with k simply being the diameter of the individual sandgrains. The results from Nikuradse's experiments have been used to explain the behavior of generic, naturally occurring surface roughness. This is evidenced by the widespread use of the equivalent sandgrain height, k_s. This parameter is defined as the sandgrain height in Nikuradse's experiment that has the same roughness function in the fully-rough regime as the surface of interest. The use of k_s is attractive because it is simple, but is also problematic because it is not physically related to the surface roughness profile for generic surfaces of engineering interest. Most naturally occurring rough surfaces do not behave like Nikuradse sand surfaces.

Contributed by the Fluids Engineering Division for publication in the JOURNAL OF FLUIDS ENGINEERING. Manuscript received by the Fluids Engineering Division August 14, 2001; revised manuscript received December 31, 2001. Associate Editor: T. Gatski.

Colebrook [14] first demonstrated this in a study of the irregular surface roughness in pipes resulting from the manufacturing process.

Nikuradse's roughness function for uniform sand roughness has led to the critical roughness height concept. This concept states there exists some critical roughness height for surfaces below which there is no increase in drag. This is termed the hydrodynamically smooth condition. In this condition the individual roughness elements are small enough to be completely submerged in the viscous sublayer region of the boundary layer. In order to have a hydrodynamically smooth surface, k^+ must be less than a critical value ranging from 2.25 to 5. For this surface type, if the viscous length scale is known, a critical roughness height may be specified for a surface below which a reduction in roughness height causes no concomitant reduction in drag. A recent paper by Bradshaw [15] questions the existence of a critical roughness height on theoretical grounds. He argues that the roughness function should go asymptotically to 0 in the limit as k^+ goes to 0.

Granville [16] offers three alternative methods for determining the roughness function of a surface experimentally using pipe flow, towed flat plates, and rotating disks, respectively. The procedure given for towed flat plates was used in the present investigation to determine the roughness function. Further details are given in the Results and Discussion section of the paper. It should be noted that ΔU^+ can also be obtained directly by measuring the mean velocity profile over a rough wall. Once $\Delta U^+ = \Delta U^+(k^+,[l])$ for a surface is known, it can be used in a boundary layer code or a similarity law analysis to predict the drag of any body covered with that roughness.

A great deal of effort has been made to correlate the roughness function for a surface with its roughness statistics. This would allow the drag change to be predicted based on knowledge of the surface profile alone. However, development of a universal relationship to correlate the roughness function to the surface roughness length scales has been illusive. Several researchers have attempted to correlate the roughness function with a roughness height and density parameter for relatively simple uniform roughness [17,18]. Koch and Smith [19] and Acharya et al. [12] both looked at the effect of machined roughness on frictional resistance. Acharya et al. found that collapsing the roughness functions for these surfaces to a universal curve using R_a alone was not possible and suggested that the deviation in the slope angles of the roughness might allow better correlation. Both Townsin et al. [7] and Musker [8] have proposed correlations that include roughness height as well as texture. Townsin proposed that a height parameter, *h*, based on the first three even moments of the profile power spectral density reasonably collapsed the roughness functions for ship hull surfaces. Townsin and Dey [20] give the following formulation for the roughness function of ship hull coatings based on their modified roughness Reynolds number:

$$\Delta U^+ = \frac{1}{\kappa}\ln(1+0.18h^+) \tag{4}$$

where

$$h = \sqrt{\alpha m_0 m_2}$$

$$\alpha = \frac{m_o m_4}{m_2^2} \tag{5}$$

$$m_n = \int_{2\pi/Lp}^{\pi/Ls} E\gamma^n d\gamma$$

Musker [8] suggests an alternative roughness scale that incorporates the skewness and kurtosis of the roughness height distribution. Grigson [6] asserts that the statistics of the surface profile alone cannot be relied upon to predict the roughness function. He contends that only experimental testing of the surface of interest allows accurate determination of the roughness function. It is of note that Grigson's results indicate that the roughness functions of some ship hull coatings do not behave as either Nikuradse or Colebrook-type functions and may have multiple inflection points.

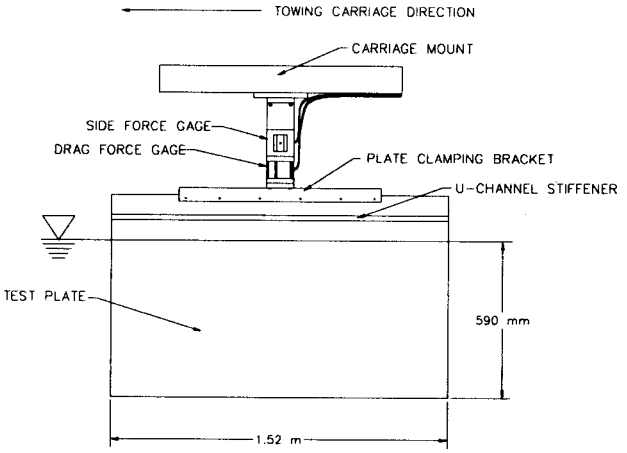

Fig. 1 Schematic of the flat plate test fixture

The goal of the present experimental investigation is to document the frictional resistance and surface roughness of a range of sanded paint surfaces. An attempt to identify a suitable roughness parameter relating the physical roughness and the roughness function for this particular class of surfaces is made. The results are then scaled up to a planar surface using the similarity law procedure of Granville [21] to predict the effect of the present roughness on the frictional resistance of a plate of the order of length of typical sailing vessels.

Experimental Facilities and Method

The present experiments were conducted in the 115 m long towing tank facility at the United States Naval Academy Hydromechanics Laboratory. The width and depth of the tank are 7.9 m and 4.9 m, respectively. The towing carriage has a velocity range of 0–7.6 m/s. In the present investigation the towing velocity was varied between 2.0 m/s–3.8 m/s ($\mathrm{Re}_L = 2.8\times10^6 - 5.5\times10^6$). The velocity of the towing carriage was measured and controlled using an encoder on the rails that produce 4000 pulses/m. Using this system, the precision uncertainty in the mean velocity measurement was $<0.02\%$ over the entire velocity range tested. The working fluid in the experiments was fresh water, and the temperature was monitored to within ±0.05°C during the course of the experiments using a thermocouple with digital readout. Further details of the experimental facility are given in [22].

Figure 1 shows a schematic of the test fixture and plate. The flat test plate was fabricated from 304 stainless steel sheet stock and measured 1.52 m in length, 0.76 m in width, and 3.2 mm in thickness. Both the leading and trailing edges were filleted to a radius of 1.6 mm. No tripping device was used to stimulate transition. The overall drag of the plate was measured using a Model HI-M-2, modular variable-reluctance displacement force transducer manufactured by Hydronautics Inc. An identical force transducer, rotated 90 deg to drag gage, was included in the test rig to measure the side force on the plate. The purpose of the side force gage was to ensure precise alignment of the plate. This was accomplished by repeatedly towing the plate at a constant velocity and adjusting the yaw angle of the test fixture to minimize the side force. Once this was done, no further adjustments were made to the alignment over the course of the experiments. The side force was monitored throughout to confirm that the plate alignment did not vary between test surfaces. Both of the force transducers used in the experiments had load ranges of 0–89 N. The combined bias uncertainty of the gages is $\pm0.25\%$ of full scale. Data were gathered at a sampling rate of 100 Hz and were digitized using a

16-bit A/D converter. The length of the towing tank dictated the sampling duration. This ranged from ~30 s of data per test run at the lowest Reynolds number to ~11 s of at the highest Reynolds number. The overall drag was first measured with 590 mm of the plate submerged. This was repeated with 25 mm of the plate submerged in order to find the wavemaking resistance tare. The difference between the two was taken to be the frictional resistance on the two 565 mm wide by 1.52 m long faces of the plate. The tests were repeated ten times for each surface and velocity. The results presented are the means of these runs.

A single test plate was used for all the towing experiments. This was done to ensure that any differences in the drag measured were due to the surface condition of the plate and not small variations in leading edge shape, plate flatness, and other factors that could have varied between multiple test plates. The plate was initially painted with several coats of marine polyamide epoxy paint manufactured by International Paint. This surface condition was termed the ''unsanded'' condition. After hydrodynamic testing, the plate was wet sanded with 60-grit sandpaper. This surface was referred to as the ''60-grit sanded'' condition. Subsequent to hydrodynamic testing under the 60-grit sanded condition, the entire process was repeated for the ''120-grit sanded,'' ''220-grit sanded,'' ''400-grit sanded,'' and ''600-grit sanded'' surface conditions. After hydrodynamic testing of the 600-grit sanded surface the plate was wet sanded up to 1800 grit and polished with a buffing wheel using Maquire's swirl remover polishing compound. This surface is referred to as the ''polished'' condition. All the sanding in the present experiment was carried out by hand with the aid of a sanding block using small circular motions. Prussian blue was used to dye the surface before sanding with finer grit paper to ensure the entire surface was sanded and to reveal the surface scratches left behind by the previous grit so they could be removed. The surfaces were cleaned with water and a soft cloth between surface treatments to remove grit and detritus left behind by the sanding process.

The surface profiles of the test plates were measured using a Cyber Optics laser diode point range sensor (model #PRS 40) laser profilometer system mounted to a Parker Daedal (model #106012BTEP-D3L2C4M1E1) two-axis traverse with a resolution of 5 μm. The resolution of the sensor is 1 μm with a laser spot diameter of 10 μm. Data were taken over a sampling length of 50 mm and were digitized at a sampling interval of 25 μm. Ten linear profiles were taken on each of the test surfaces. A single three-dimensional topographic profile was made on each of the surfaces by sampling over a square area 2.5 mm on a side with a sampling interval of 25 μm.

The roughness statistics were calculated using the linear profiles from each of the surfaces. All were calculated without using a long wavelength cutoff (effectively the cutoff was the sampling length, 50 mm) and using 25 mm, 10 mm, 5 mm, 2 mm, and 1 mm long wavelength filters. The highpass filtering was carried out using a Butterworth digital filter and the long wavelength cutoffs were chosen to be in the range used by Musker [8] and Townsin and Dey [20]. The purpose of the filtering was to remove surface waviness which has little effect on the drag. Musker says that the long wavelength cutoff should be set equal to the size of the large energy-containing eddies near the surface, and he suggests using the Taylor macro-scale. In the present investigation no spatial turbulence correlations were available from which to calculate the Taylor macro-scale, so roughness statistics using a range of long wavelength cutoffs were calculated.

Some of the roughness statistics calculated for the surfaces included the centerline average height, R_a, given as:

$$R_a = \frac{1}{N}\sum_{i=1}^{N} |y_i| \tag{6}$$

It should be noted that all of the roughness statistics are calculated using the centerline as the datum for y. This is defined as the datum at which the average value of y is zero. R_q is the root mean square height given as:

$$R_q = \sqrt{\frac{1}{N}\sum_{i=1}^{N} y_i^2} \tag{7}$$

R_t is the height from the called maximum peak to the minimum trough and is given as:

$$R_t = y_{\max} - y_{\min} \tag{8}$$

R_z is called the ten point height and is given as the mean of the difference of the five highest peaks and the five lowest troughs.

$$R_z = \frac{1}{5}\sum_{i=1}^{5} (y_{\max i} - y_{\min i}) \tag{9}$$

The correlation length scale, λ_{corr}, is calculated as the distance (j times the sampling interval, L_p) at which the autocorrelation function falls below 0.5. The autocorrelation function is given by:

$$C_j = \frac{\dfrac{1}{N-1-j}\displaystyle\sum_{i=1}^{N-1-j} (y_i y_{i+j})}{\dfrac{1}{N-1}\displaystyle\sum_{i=1}^{N} y_i^2} \tag{10}$$

It should be noted that for the 120-grit and smoother surfaces this value was less than the sampling interval so no accurate estimate could be made. The root mean square slope, sl_{rms}, is given as follows:

$$sl_{rms} = \sqrt{\frac{1}{N-1}\sum_{i=1}^{N-1} \left\{\frac{(y_{i+1}-y_i)}{(x_{i+1}-x_i)}\right\}^2} \tag{11}$$

A similar parameter, the root mean square slope angle, was offered by Acharya et al. [12] as an important one in describing roughness caused by machining on turbine blades. By calculating the power spectral density of the surface waveforms using a fast Fourier transform and the first three even moments of the power spectral density, Townsin's height parameter, h, was calculated using Eq. (4). Musker [8] offers an alternative roughness length scale given by:

$$h' = R_q(1 + aS_p)(1 + bS_k K_u) \tag{12}$$

His results show that this roughness length scale works well for correlating the roughness function for a range of ship hull coatings when a long wavelength cutoff of 2 mm is used and the constants a and b are taken to be 0.5 and 0.2, respectively.

Uncertainty Estimates

Precision uncertainty estimates for the resistance measurements were made through repeatability tests using the procedure given by Moffat [23]. Ten replicate experiments were made with each of the test plates at each Reynolds number. This was carried out so that the relatively small differences in the frictional resistance between the surface conditions could be identified. The standard error for C_F was then calculated. In order to estimate the 95% precision confidence limits for a mean statistic, the standard error was multiplied by the two-tailed t value ($t = 2.262$) for 9 degrees of freedom, as given by Coleman and Steele [24]. The resulting precision uncertainties in C_F were $\leqslant \pm 0.3\%$ for all the tests. The overall precision and bias error was dominated by the systematic error due to the combined bias of the force gages ($\pm 0.25\%$ full scale). The resulting overall precision and bias uncertainty in C_F ranged from $\pm 4.8\%$ at the lowest Reynolds number to $\pm 1.4\%$ at the highest Reynolds number. Periodically throughout the experiments, a reference plate was run to check that the resulting mean C_F value was within the precision uncertainty bounds that had been obtained from previous testing with the same surface. This

Table 1 Roughness statistics

Specimen	λ_{FL} (mm)	R_a (μm)	R_q (μm)	R_t (μm)	R_z (μm)	S_k	K_u	λ_{corr} (μm)	sl_{rms}	h (μm)
Unsanded	NF	2.7 ± 0.2	5.0 ± 0.3	39 ± 2	38 ± 2	2.0 ± 0.2	5.0 ± 0.3	127 ± 22	0.113 ± 0.006	2.2 ± 0.3
	10	3.4 ± 0.2	4.8 ± 0.3	50 ± 3	43 ± 3	0.02 ± 0.1	4.8 ± 0.3	118 ± 9	0.113 ± 0.006	2.1 ± 0.3
	1	2.5 ± 0.1	3.4 ± 0.2	28 ± 2	25 ± 2	-0.01 ± 0.1	3.4 ± 0.2	31 ± 1.7	0.112 ± 0.006	1.0 ± 0.1
60-Grit	NF	0.96 ± 0.06	1.63 ± 0.09	12 ± 1.6	11 ± 0.9	1.1 ± 0.1	3.2 ± 0.4	40 ± 7	0.063 ± 0.002	0.24 ± 0.01
	10	1.14 ± 0.07	1.62 ± 0.08	13 ± 1.6	11 ± 0.9	0.61 ± 0.1	2.1 ± 0.5	31 ± 6	0.063 ± 0.002	0.24 ± 0.01
	1	1.05 ± 0.05	1.43 ± 0.07	13 ± 2	11 ± 0.6	-0.21 ± 0.1	1.5 ± 0.2	<25*	0.063 ± 0.002	0.19 ± 0.01
120-Grit	NF	0.58 ± 0.03	1.02 ± 0.04	9.4 ± 0.7	7.6 ± 0.2	1.4 ± 0.2	5.2 ± 1.1	<25*	0.047 ± 0.002	0.10 ± 0.005
	10	0.70 ± 0.02	1.01 ± 0.03	10 ± 0.95	8.1 ± 0.3	0.96 ± 0.09	4.0 ± 1.0	<25*	0.047 ± 0.002	0.10 ± 0.005
	1	0.65 ± 0.03	0.90 ± 0.03	9.2 ± 0.6	7.7 ± 0.2	0.11 ± 0.08	2.5 ± 0.6	<25*	0.047 ± 0.002	0.08 ± 0.005
220-Grit	NF	0.47 ± 0.01	0.86 ± 0.04	8.6 ± 1.5	7.0 ± 0.7	1.8 ± 0.2	7.8 ± 1.9	<25*	0.039 ± 0.002	0.07 ± 0.006
	10	0.59 ± 0.02	0.86 ± 0.04	9.4 ± 1.6	7.7 ± 0.8	1.1 ± 0.2	5.3 ± 1.3	<25*	0.039 ± 0.002	0.07 ± 0.006
	1	0.52 ± 0.02	0.74 ± 0.04	9.1 ± 1.2	7.0 ± 0.7	0.15 ± 0.06	3.9 ± 0.8	<25*	0.039 ± 0.002	0.05 ± 0.005
400-Grit	NF	0.43 ± 0.03	0.77 ± 0.04	8.0 ± 0.5	7.0 ± 0.7	1.8 ± 0.1	8.1 ± 1.6	<25*	0.038 ± 0.001	0.06 ± 0.007
	10	0.52 ± 0.03	0.77 ± 0.04	8.6 ± 0.4	7.7 ± 0.8	1.4 ± 0.2	6.5 ± 1.3	<25*	0.038 ± 0.001	0.06 ± 0.007
	1	0.49 ± 0.03	0.70 ± 0.03	8.1 ± 0.4	7.0 ± 0.7	0.5 ± 0.2	4.3 ± 0.9	<25*	0.038 ± 0.001	0.05 ± 0.003
600-Grit	NF	0.40 ± 0.01	0.73 ± 0.02	7.9 ± 2.6	6.0 ± 0.6	2.1 ± 0.7	15 ± 14	<25*	0.038 ± 0.002	0.05 ± 0.003
	10	0.47 ± 0.02	0.73 ± 0.03	8.4 ± 2.5	6.3 ± 0.6	1.8 ± 0.7	13 ± 12	<25*	0.038 ± 0.002	0.05 ± 0.003
	1	0.47 ± 0.02	0.67 ± 0.03	9.1 ± 2.5	6.5 ± 0.9	0.5 ± 0.3	7.7 ± 6	<25*	0.038 ± 0.002	0.04 ± 0.003
Polished	NF	0.18 ± 0.004	0.30 ± 0.01	2.0 ± 0.3	1.9 ± 0.3	1.15 ± 0.08	3.3 ± 0.3	<25*	0.015 ± 0.001	0.009 ± 0.001
	10	0.21 ± 0.006	0.30 ± 0.01	2.4 ± 0.1	2.1 ± 0.4	0.70 ± 0.07	2.3 ± 0.2	<25*	0.015 ± 0.001	0.009 ± 0.001
	1	0.19 ± 0.004	0.27 ± 0.01	2.6 ± 0.1	2.2 ± 0.1	0.18 ± 0.06	2.1 ± 0.2	<25*	0.015 ± 0.001	0.007 ± 0.001

* - λ_{corr} was < L_s

All uncertainties represent the 95% confidence precision bounds for the measurement

was confirmed in all cases tested. Uncertainty estimates for the roughness statistics were calculated in the same manner and are reported in Table 1.

Results and Discussion

The presentation of the results and discussion will be organized as follows. First, a qualitative discussion of the nature of each of the surfaces tested will be made. The roughness statistics will then be presented. Next the results of the hydrodynamic tests will be presented and discussed. Finally, an attempt will be made to relate the roughness statistics of this class of surfaces to the roughness function, ΔU^+.

Qualitative Description of the Surfaces. In order to better understand the nature of each of the surfaces tested, a qualitative description of each will be made using the three-dimensional topographic profiles shown in Fig. 2. Even cursory inspection of the profiles shows that the surfaces vary greatly. Figure 2(*a*) shows the unsanded surface and indicates that it has relatively large features with a wavelength of up to 1 mm. This is very common in as-sprayed paint surfaces and is often referred to as ''orange peel'' because of the characteristic texture. Figure 2(*b*), which shows the 60-grit surface, indicates that the orange peel has been almost entirely removed by sanding, but linear scratches have been added. These scratches have a width of up to 150 μm and a depth of up to 25 μm. Figure 2(*c*) shows the 120-grit surface. Many of the scratches seen in the 60-grit surface have been removed, and narrower, shallower scratches have been added. It is of note that some of the deeper scratches from the 60-grit surface have not been completely removed and remain as features of up to 150 μm in width, with a depth of up to 10 μm. The 220-grit surface (Fig. 2(*d*)) shows that the scratches from the 60-grit paper have been removed. They have been replaced with finer scale scratches that are much narrower and shallower. The 400-grit and 600-grit surfaces are very similar in nature and for this reason only the 600-grit surface (Fig. 2(*e*)) is presented. The polished surface (Fig. 2(*f*)) shows that many of the small scale peaks and troughs seen in the 400-grit and 600-grit surfaces have been removed.

The evolution of the surface scratches can be more easily seen in plan views of the previous figures. These views for the unsanded, 60-grit, 120-grit, and 220-grit surfaces are given in Fig. 3. Figure 3(*a*) of the unsanded specimen shows the orange peel surface. The 60-grit surface (Fig. 3(*b*)) shows that the orange peel has been removed and linear scratches have been added. Smaller scale scratches are evident in the 120-grit surface (Fig. 3(*c*)) as well as 60-grit scratches that have not been completely removed. By the time the 220-grit paper has been used (Fig. 3(*d*)), only rather small scale features remain.

The quantitative statistics of the roughness surfaces are given in Table 1. The results are presented for processing with no long wavelength filter, a 10 mm long wavelength filter, and a 1 mm long wavelength filter. One item of note is that all of the roughness tested in the present study is quite small compared to the roughness used in a majority of previous studies. Most basic research has focused on roughness large enough to generate turbulent flows in the fully-rough regime, and the studies on ship hull roughness by Musker [8] and others addressed smaller scale transitional roughness with 150 μm$\leqslant R_t \leqslant$600 μm ($5 \leqslant k^+ \leqslant 320$; k^+ based on R_t). For the present study, the range of roughness was 2 μm$\leqslant R_t \leqslant$39 μm ($0.15 \leqslant k^+ \leqslant 5$; k^+ based on R_t). This is important to keep in mind because the differences in drag for the surfaces is expected to be rather small. The change in the roughness statistics for the unfiltered profiles with sanding is shown in Fig. 4. The figure shows that all of the roughness height parameters are reduced with sanding up to 220-grit. At that point, no significant reduction in the roughness height is made by sanding with 400-grit and 600-grit. The polished surface does show a significant reduction in roughness. Figure 2(*f*) shows that this is largely due to a reduction in the isolated protuberances seen in the 220-grit, 400-grit, and 600-grit surfaces.

Test Results. The results of the hydrodynamic tests are shown in Fig. 5. The Schoenherr mean line for smooth plates is shown for comparison [25]. The Schoenherr mean line is given as:

$$\frac{0.242}{\sqrt{C_F}} = \log(\mathrm{Re}_L C_F) \tag{13}$$

Table 2 shows the % increase in C_F for the test surfaces compared to the polished surface. The results show that the 60-grit specimen had a significant reduction in C_F from the unsanded surface. A further reduction in C_F was found for the 120-grit specimen compared with the 60-grit surface. A smaller, but significant, reduction in C_F occurred for the 220-grit surface compared with the 120-grit specimen. However, no significant change in C_F was seen for the 400-grit and 600-grit surfaces compared to the 220-grit surface. Inspection of Figs. 2(*d*–2*e*) and Table 1 shows that the roughness on these surfaces is quite similar as well. The polished surface had C_F values that were significantly less than any of the other specimens. The reduction in frictional resistance seems to be due to a reduction in the isolated protuberances (Fig. 2(*f*)) that were seen in the 600-grit surface (Fig. 2(*e*)).

It should be noted that the results could have been affected to varying degree by the influence of the surface roughness and Reynolds number on the transition of the flow to turbulence. The flow was not tripped, so the transition point may have varied between the test cases depending on the surface roughness. Leading-edge and three-dimensional effects could have also had some influence on these results. However, these effects are very difficult to quantify precisely. Overall, it is felt these effects are small since the smooth plate results agree within ~1% with the Schoenherr mean line for frictional resistance in turbulent flow. The fact that the smooth plate results remain a fairly constant percentage lower than the Schoenherr mean line over the range of Reynolds number tested seems to also indicate that the transition point must not vary significantly over the Reynolds number range tested.

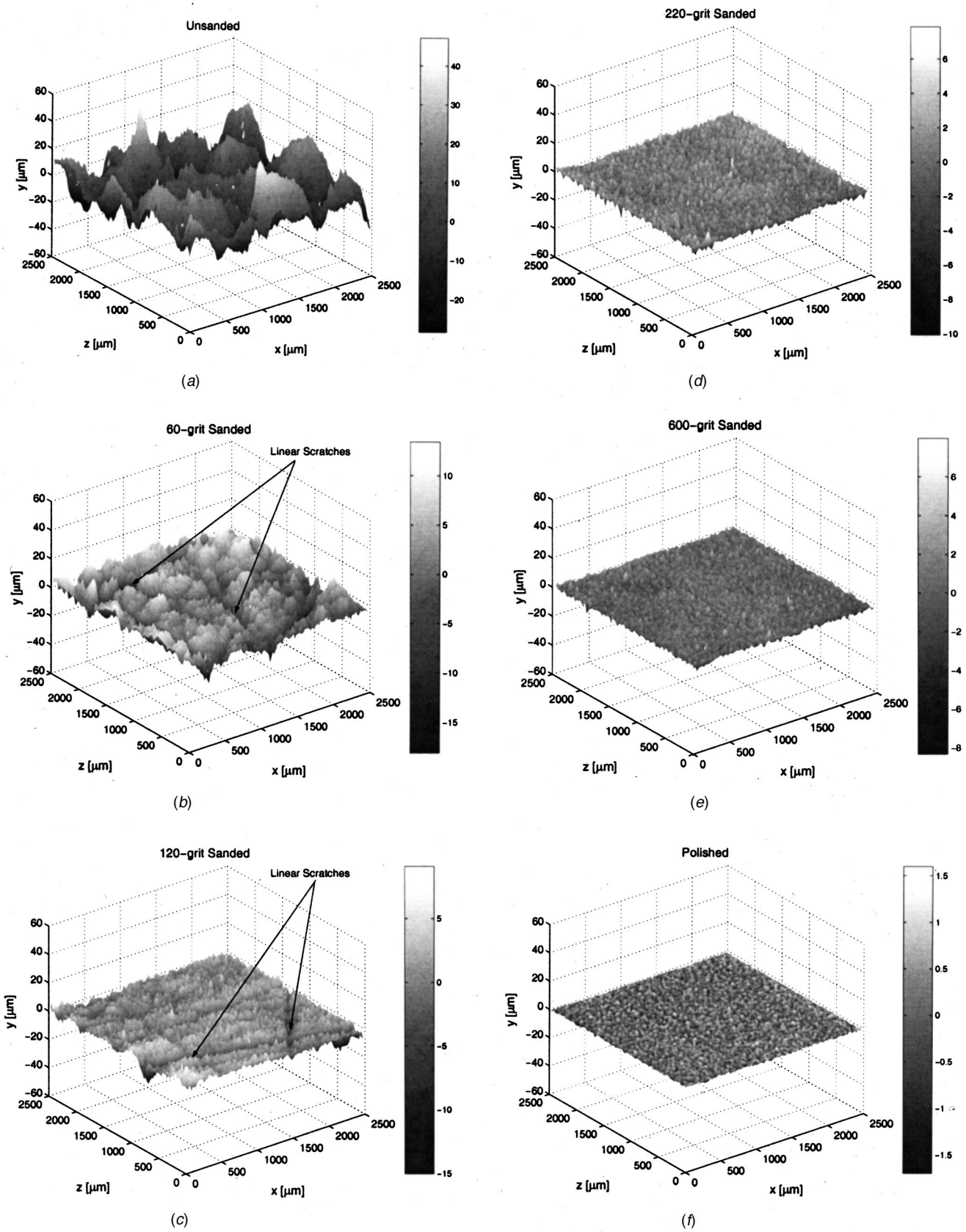

Fig. 2 Surface waveforms for (*a*) the unsanded specimen, (*b*) the 60-grit specimen, (*c*) the 120-grit specimen, (*d*) the 220-grit specimen, (*e*) the 600-grit specimen, and (*f*) the polished specimen. (Uncertainty in the y-direction ±1 μm, *x*- and *z*-directions ±5 μm)

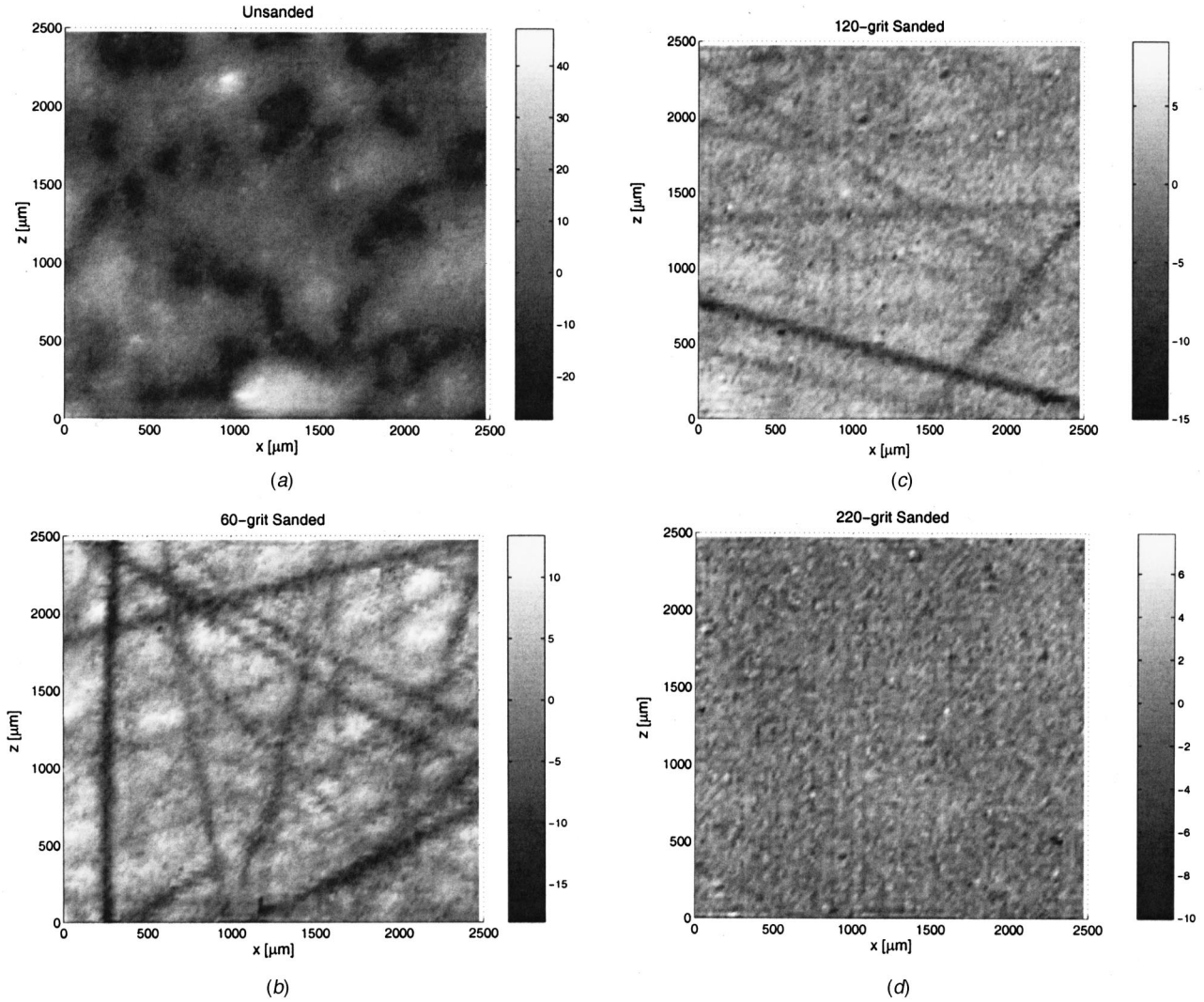

Fig. 3 Plan view of the surface waveform for (*a*) the unsanded specimen, (*b*) the 60-grit specimen, (*c*) the 120-grit specimen, and (*d*) the 220-grit specimen. (Uncertainty in the y-direction ±1 μm, *x*- and *z*-directions ±5 μm)

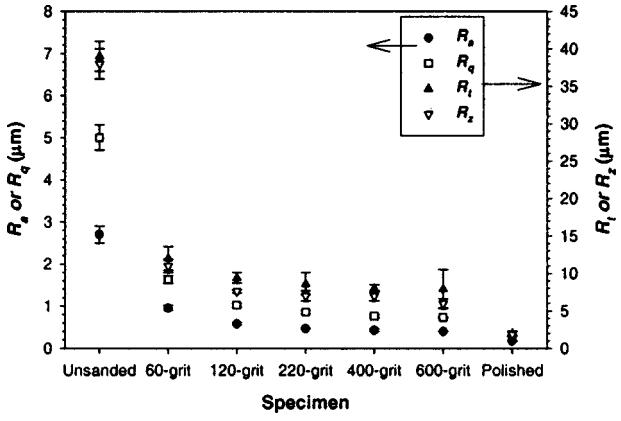

Fig. 4 The effect of sanding on the roughness statistics of the unfiltered profiles. (Error bars represent the 95% confidence limits for the precision uncertainty.)

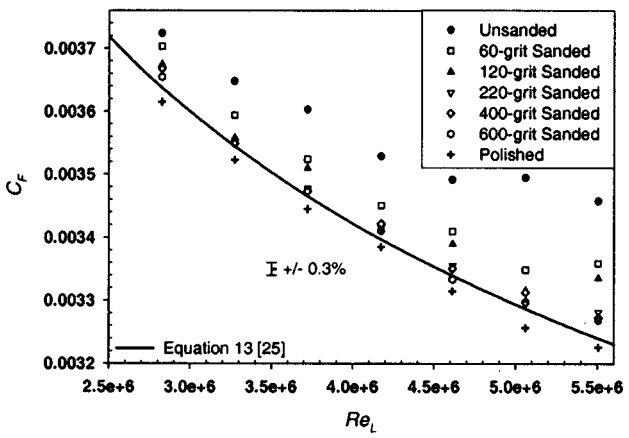

Fig. 5 Overall frictional resistance coefficient versus Reynolds number for all the specimens. (Precision uncertainty ≤±0.3% at all Reynolds numbers; overall precision and bias ranges from ±1.4% at highest Reynolds number to ±4.8% at lowest Reynolds number.)

Table 2 Increase in overall frictional resistance coefficient for the test specimens compared to the polished surface

Specimen	Average % Increase in C_F	Range of % Increase in C_F
Unsanded	5.0	3.0 – 7.3
60-Grit	2.6	2.0 – 4.1
120-Grit	1.9	1.0 – 3.4
220-Grit	1.2	0.8 – 1.7
400-Grit	1.2	0.7 – 1.7
600-Grit	1.0	0.6 – 1.4

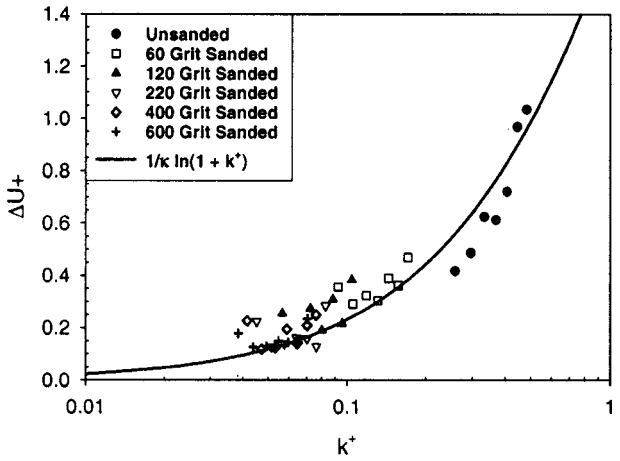

Fig. 6 Roughness function for all specimens. (Overall uncertainty ±0.1 in ΔU^+)

Relation of Roughness Statistics to ΔU^+. Using similarity law analysis, Granville [16] derived an expression to relate the local frictional coefficient, c_f, at the trailing edge of a planar surface to the overall frictional resistance coefficient, C_F, for the same surface. It is given as:

$$\left(\sqrt{\frac{c_f}{2}}\right)_{TE} = \left(\frac{U_\tau}{U_e}\right)_{TE} = \sqrt{\frac{C_F}{2}}\left(1-\kappa\sqrt{\frac{C_F}{2}}\right) \tag{14}$$

By solving this equation for U_τ, the viscous length scale, ν/U_τ, at the trailing edge of the plate can be obtained. For the present surfaces ν/U_τ ranged from $\sim$14 μm at $\mathrm{Re}_L = 2.8\times10^6$ to $\sim$7.6 μm at $\mathrm{Re}_L = 5.5\times10^6$. The roughness function, ΔU^+, at the trailing edge of the plate can be found using the method of Granville [16] as well. This procedure involves plotting $\sqrt{2/C_F}$ versus $\mathrm{Re}_L C_F$. The roughness function, ΔU^+, is given as the following evaluated at the same value of $\mathrm{Re}_L C_F$ for both smooth and rough walls:

$$\Delta U^+ = \left(\sqrt{\frac{2}{C_F}}\right)_S - \left(\sqrt{\frac{2}{C_F}}\right)_R \tag{15}$$

In the present study, the results for the polished surface were used as smooth plate values. Since the behavior of ΔU^+ at vanishing roughness height did not behave as a Nikuradse-type roughness function, attempts were made to collapse the results to a Colebrook-type roughness function as given by:

$$\Delta U^+ = \frac{1}{\kappa}\ln(1+k^+) \tag{16}$$

All of the roughness length scales in Table 1 were considered including the Musker [8] and Townsin [20] length scales. The best fit of the results to Eq. (16) was obtained using a multiple of the centerline average height, R_a, calculated from the unfiltered profiles as k. With $k = 1.35R_a$, 87% of the variance (i.e., $R^2 = 0.87$) in ΔU^+ could be explained with the Colebrook-type roughness function (Eq. (16)). The results are shown in Fig. 6. It should be noted that >80% of the variance could also be explained for this relatively simple roughness using R_q, R_t, or R_z calculated from the unfiltered profiles. Attempts to use the filtered profile statistics led to larger scatter in the roughness function than the unfiltered profile statistics. This seems to indicate that for sanded surfaces in this Reynolds number range, long wavelength roughness (up to 50 mm) contributes significantly to the increase in frictional resistance.

Using the roughness function obtained for a flat plate, Granville [16] gives a similarity law procedure for calculating the effect of the same roughness on a planar surface of arbitrary length. This was carried out with the present results for surfaces of 4 m and 12 m. These lengths were chosen to be representative of the range of length of sailing vessels for which sanding would be practicable. Using this analysis, significant increases in C_F above the polished plate values were predicted for the surfaces. These increases were of the same order as seen in the present experiments. For example, it was found that the unsanded surface would have an average increase in C_F of 5.0% above a polished surface over a velocity range of 2.3–4.6 m/s (4.5–8.9 knots) at a length of 4 m and an average increase in C_F of 4.5% over a velocity range of 2.6–5.0 m/s (5.1–9.7 knots) at a length of 12 m. Over the same velocity range, the 60-grit surface would have an average increase in C_F of 2.5% at a length of 4 m and an average increase in C_F of 2.3% at a length of 12 m. The increase for the 120-grit surface would be 1.9% at a length of 4 m and 1.6% at a length of 12 m. Both the 220-grit and 400-grit surfaces would have an increase of 1.3% and 1.1% at lengths of 4 m and 12 m, respectively, while the increase for the 600-grit surface would be 1.1% and 1.0% at lengths of 4 m and 12 m, respectively. Due to the three-dimensional nature of the boundary layer flow around a real vessel, however, additional data on actual hull shapes are needed to corroborate these findings. It should also be noted that in the present study significant care was given to ensure that the entire surface was sanded and that no area was missed. This was relatively easy on a small flat surface, but would be much more difficult in practice on a large three-dimensional shape.

Conclusion

Measurements of the roughness and frictional resistance of sanded paint surfaces have been made. The results indicate that as-sprayed, unsanded surfaces can have a significant increase in C_F compared to a polished surface. Smaller, but significant, increases in C_F compared to the polished surface were also noted on surfaces sanded with sandpaper as fine as 600-grit. This increase seems to be due to isolated surface protuberances not completely removed by the sanding process. The roughness function, ΔU^+, shows good collapse to a Colebrook-type roughness function for this class of surfaces when a multiple of the centerline average height ($k = 1.35R_a$) is used as the roughness length scale. Similarity law predictions of C_F on larger planar surfaces of sailing vessel length show that similar increases in C_F can be expected in that range of wetted length as well. Further effort needs to be focused on understanding the effect of roughness on three-dimensional bodies.

Acknowledgments

I would like to thank the Office of Naval Research for financial support under the direction of Dr. Steve McElvaney. Many thanks go to Mr. Steve Enzinger, Mr. Don Bunker, and the rest of the USNA Hydromechanics Lab staff for their valuable help in providing technical support. I also thank Mr. Bill Beaver of the USNA Technical Support Division who provided a great deal of practical insight and never seemed to tire of sanding. I am grateful to Prof. Peter Bradshaw, Prof. Karen Flack, Prof. Ralph Volino, and the anonymous reviewers for reading drafts of the manuscript and offering many helpful comments. I am also indebted to Prof. Michelle Koul for helping with the laser profilometry.

Nomenclature

a, b = constants in Musker's roughness length scale equation
B = smooth wall log-law intercept = 5.0
C_F = overall frictional resistance coefficient = $(F_D)/(1/2\rho U_e^2 S)$
c_f = local frictional resistance coefficient = $(\tau_o)/(1/2\rho U_e^2)$
C_j = autocorrelation function
E = power spectral density of surface waveform
F_D = drag force
h = Townsin's roughness height parameter = $\sqrt{\alpha m_0 m_2}$
j = lag in autocorrelation function
k = arbitrary measure of roughness height
k_s = sand roughness height or equivalent sand roughness height
K_u = kurtosis
L = plate length
L_p = overall length of surface profile
L_s = profile sampling interval
$[l]$ = other roughness length scales
m_n = nth moment of the power spectral density
N = number of samples in surface profile
Re_{δ^*} = displacement thickness Reynolds number = $U_e \delta^* / \nu$
Re_L = Reynolds number based on plate length = $U_e L / \nu$
R_a = centerline average roughness height = $(1/N)\Sigma_{i=1}^{N} |y_i|$
R_q = root mean square roughness height = $\sqrt{(1/N)\Sigma_{i=1}^{N} y_i^2}$
R_t = maximum peak to through height = $y_{\max} - y_{\min}$
R_z = ten point roughness height = $\Sigma_{i=1}^{5} (y_{\max i} - y_{\min i})$
S = wetted surface area
sl_{rms} = root mean square slope of the roughness profile = $\sqrt{(1/N-1)\Sigma_{i=1}^{N-1} \{(y_{i+1}-y_i)/(x_{i+1}-x_i)\}^2}$
S_k = skewness
S_p = average absolute slope of roughness profile
U = mean velocity in the x direction
U_e = freestream velocity relative to surface
ΔU^+ = roughness function
U_τ = friction velocity = $\sqrt{\tau_o / \rho}$
x = streamwise distance from plate leading edge
y = normal distance from the boundary measured from roughness centerline
α = bandwidth parameter = $m_0 m_4 / m_2^2$
δ = boundary layer thickness
δ^* = displacement thickness = $\int_0^\delta (1 - U/U_e) dy$
κ = von Karman constant = 0.41
γ = wavenumber = $2\pi/\lambda$
λ = wavelength
λ_{corr} = correlation length scale
ν = kinematic viscosity of the fluid
Π = wake parameter
ρ = density of the fluid
τ_o = wall shear stress
ω = wake function

Superscript

$+$ = inner variable (normalized with U_τ or U_τ / ν)

Subscript

FL = long wavelength filter
min = minimum value
max = maximum value
R = rough surface
S = smooth surface
TE = trailing edge

References

[1] Nikuradse, J., 1933, "Laws of Flow in Rough Pipes," *NACA Technical Memorandum 1292*.
[2] Hama, F. R., 1954, "Boundary-Layer Characteristics for Rough and Smooth Surfaces," Transactions SNAME, **62**, pp. 333–351.
[3] Ligrani, P. M., and Moffat, R. J., 1986, "Structure of Transitionally Rough and Fully Rough Turbulent Boundary Layers," J. Fluid Mech., **162**, pp. 69–98.
[4] Krogstad, P. Å., and Antonia, R. A., 1992, "Comparison Between Rough-and Smooth-Wall Turbulent Boundary Layers," J. Fluid Mech., **245**, pp. 599–617.
[5] Raupach, M. R., Antonia, R. A., and Rajagopalan, S., 1991, "Rough-Wall Turbulent Boundary Layers," Appl. Mech. Rev., **44**, No. 1, 1991, pp. 1–25.
[6] Grigson, C. W. B., 1992, "Drag Losses of New Ships Caused by Hull Finish," J. Ship Res., **36**, No. 2, pp. 182–196.
[7] Townsin, R. L., Byrne, D., Svensen, T. E., and Milne, A., 1981, "Estimating the Technical and Economic Penalties of Hull and Propeller Roughness," Transactions SNAME, **89**, pp. 295–318.
[8] Musker, A. J., 1980–1981, "Universal Roughness Functions for Naturally-Occurring Surfaces," Trans. Can. Soc. Mech. Eng., **1**, pp. 1–6.
[9] Lewkowicz, A. K., and Musker, A. J., 1978, "The Surface Roughness on Ship Hulls: Interaction in the Viscous Sublayer," *Proceedings of the International Symposium on Ship Viscous Resistance-SSPA Goteborg, Sweden*.
[10] *Proceedings of the RINA International Workshop on Marine Roughness and Drag*, 1990, London, UK.
[11] Clauser, F. H., 1954, "Turbulent Boundary Layers in Adverse Pressure Gradients," J. Aeronaut. Sci., **21**, pp. 91–108.
[12] Acharya, M., Bornstein, J., and Escudier, M. P., 1986, "Turbulent Boundary Layers on Rough Surfaces," Exp. Fluids, **4**, pp. 33–47.
[13] Perry, A. E., and Li, J. D., 1990, "Experimental Support for the Attached-Eddy Hypothesis in Zero-Pressure Gradient Turbulent Boundary Layers," J. Fluid Mech., **218**, pp. 405–438.
[14] Colebrook, C. F., 1939, "Turbulent Flow in Pipes with Particular Reference to the Transition between Smooth and Rough Pipe Laws," Journal of Civil Engineers, **11**, pp. 133–157.
[15] Bradshaw, P., 2000, "A Note on 'Critical Roughness Height' and 'Transitional Roughness'," Phys. Fluids, **12**, pp. 1611–1614.
[16] Granville, P. S., 1978, "Similarity-Law Characterization Methods for Arbitrary Hydrodynamic Roughnesses," David Taylor Naval Ship R&D Center Report 78-SPD-815-01.
[17] Betterman, R. J., 1966, "Contribution a L'etude de la Convection Forcee Turbulente le Long de Plaques Rugueuses," Int. J. Heat Mass Transf., **9**, pp. 153–164.
[18] Dvorak, F. A., 1969, "Calculation Turbulent Boundary Layers on Rough Surfaces in Pressure Gradient," AIAA J., **7**, pp. 1752–1759.
[19] Koch, C. C., and Smith, L. H., 1976, "Loss Sources and Magnitudes in Axial-Flow Compressors," ASME J. Eng. Power, **98**, pp. 411–424.
[20] Townsin, R. L. and Dey, S. K., 1990, "The Correlation of Roughness Drag with Surface Characteristics," *Proceedings of the RINA International Workshop on Marine Roughness and Drag*, London, UK.
[21] Granville, P. S., 1958, "The Frictional Resistance and Turbulent Boundary Layer of Rough Surfaces," J. Ship Res., **1**, pp. 52–74.
[22] Anon, 1981, "United States Naval Academy Hydromechanics Laboratory," Catalog of Facilities from the *Proceedings of the 16th International Towing Tank Conference*, Leningrad, USSR.
[23] Moffat, R. J., 1988, "Describing the Uncertainties in Experimental Results," Exp. Therm. Fluid Sci., **1**, pp. 3–17.
[24] Coleman, H. W., and Steele, W. G., 1995, "Engineering Application of Experimental Uncertainty Analysis," AIAA J., **33**, No. 10, pp. 1888–1896.
[25] Schoenherr, K. E., 1932, "Resistances of Flat Surfaces Moving Through a Fluid," Transactions SNAME, **40**, pp. 279–313.